https://doi.org/10.1016/j.istruc.2024.105953

Stress-strain modelling for FRP-confined engineered cementitious composites under cyclic axial compression

Shuai Li, Tak-Ming Chan*, Ben Young

Department of Civil and Environmental Engineering, The Hong Kong Polytechnic University, Hong Kong, China

*Corresponding author.

Email address: tak-ming.chan@polyu.edu.hk (T.-M. Chan).

Abstract

As a high-performance building material, engineered cementitious composites (ECC) presents good ductility and toughness with strain hardening behaviour, multiple cracking behaviour and large tensile strain capacity under tensile loading, compared with normal concrete. On the other hand, ECC also shows the similar brittle failure to normal concrete in terms of compressive behaviour. Adopting fibre-reinforced polymer (FRP) confinement is an effective approach to improve the compressive strength, strain and axial deformation ductility of ECC. The current investigations on FRP-confined ECC including experimental tests as well as analytical and design modelling are mainly focused on the monotonic loading, while cyclic model for FRP-confined ECC is not available in the literature. Understanding the behaviour of FRP-confined ECC under cyclic loading is also of vital importance, especially that FRP-confined ECC is usually used in seismic retrofitting. Therefore, this study focuses on the development of stress-strain model of FRP-confined ECC under cyclic compression. Test database for FRP-confined ECC was firstly collected, followed by the assessment of the existing cyclic models developed for FRP-confined normal concrete. New equations were also developed based on the test results of FRP-confined ECC. Different components in the cyclic model, including envelope curve, unloading/reloading curves, plastic strains and stress deterioration, were discussed in detail. Finally, two cyclic models, Model I and Model II, were proposed to predict the cyclic stress-strain behaviour of FRP-confined ECC. Close agreements between the predicted curves by Model I and test curves can be obtained, indicating that Model I has good prediction performance and can be adopted to provide design guidance for FRP-confined ECC under cyclic axial compression.

Keywords: Engineered cementitious composites (ECC); Fibre-reinforced polymer (FRP); Confinement; Compressive behaviour; Cyclic stress-strain model

1. Introduction

Engineered cementitious composites (ECC) is regarded as a type of high-performance fibre-reinforced cementitious material [1-3]. Due to the fibres in the mixture, ECC can achieve distinctive enhanced tensile ductility compared with normal concrete [4]. Due to the fibre-bridging effect through the microcracks, the width of tensile cracks in ECC can be controlled and prevented from continuing growing, which leads to the multiple cracking behaviour [5]. In recent years, ECC has been widely used in various engineering applications to improve the performance of different structural members. Qin et al. [6] found that ECC was effective to enhance the flexural behaviour of reinforced concrete beams. Yang et al. [7] adopted ECC layer as the matrix for the CFRP grid external reinforcement at the bottom of reinforced concrete beam and proved that the strengthening system could achieve reliable performance. Al-Gemeel and Zhuge [8] used textile reinforced ECC to provide lateral confinement for concrete columns. Lee et al. [9] and Khan et al. [10,11] proposed the ECC-concrete encased steel composite columns and noted that ECC contributed to a more ductile failure mode and increased the overall compressive behaviour. Li et al. [12] proposed a composite column consisting of an ECC layer between outer FRP tube and inner high strength concrete (HSC) core and noticed that the ECC layer could realise a more uniform hoop strain distribution and confinement in the FRP-confined HSC composite column with enhanced deformability [12-16]. Meanwhile, ECC has also been used in the beam-column joints to improve the energy absorption ability of the plastic zone under seismic loadings [17,18]. These applications show that with the replacement of normal concrete by ECC in the crucial regions in the structural member, targeted enhancement of the structural performance can be effectively achieved. With the good cracking behaviour, ECC cover can also protect the inner reinforcements from corrosion in a better manner than normal concrete cover, which is cost-effective from the life-cycle perspective.

Though the tensile performance of ECC is prominent, its compressive behaviour is similar to normal concrete and will endure the brittle failure as well when reaching the peak strength [19,20]. Adopting fibre-reinforced polymer (FRP) lateral confinement is an effective approach to improve the compressive performance of ECC.

Dang et al. [21] and Li et al. [22] experimentally investigated the compressive behaviour of FRP-confined ECC cylinders. It was noted that both the compressive strength and strain could be obviously enhanced with the typical strain hardening performance. Yuan et al. [23,24] investigated the dilation behaviour and size effect of FRP-confined ECC stub columns. Except for conventional FRP materials, Yuan et al. [23,24] and Jiang et al. [25] also used large rupture strain (LRS) FRP materials as the lateral confinement and observed that the LRS FRP-confined ECC could achieve excellent deformability and energy dissipation capacity. With the obtained test results, design models that can predict the ultimate conditions as well as analytical models that can predict the compressive stress-strain curves have also been developed accordingly for FRP-confined ECC [21-26].

Apart from the monotonic loading, ECC could also be subjected to various more complicated loading conditions, like cyclic and seismic loadings [27]. Therefore, understanding the cyclic compressive performance of FRP-confined ECC is of vital importance, especially due to the fact that ECC and FRP are usually used together for seismic retrofitting [28,29]. Dang et al. [21] and Li et al. [22] investigated the behaviour of FRP-confined ECC stub columns under cyclic compression. It was noted that the envelope curve of cyclically loaded FRP-confined ECC was close to the stress-strain curve of the counterpart - monotonically loaded FRP-confined ECC, which has the same behaviour as FRP-confined normal concrete [30,31]. It was also observed that the deformability could be further enhanced for FRP-confined ECC specimens under cyclic compression [21,22]. There has been extensive research on the cyclic modelling for FRP-confined normal concrete, which can describe the unloading/reloading paths, plastic deformation and stress degradation behaviour [32-40]. To the best of the authors' knowledge, there is no cyclic stress-strain model developed for FRP-confined ECC in the literature. Meanwhile, the applicability of existing cyclic models developed for FRP-confined normal concrete to FRP-confined ECC remains to be unknown.

Therefore, this study focuses on the cyclic modelling for FRP-confined ECC. Test database was firstly collected as the basis for the model development. Typical cyclic models that were developed for FRP-confined normal concrete were then evaluated, with detailed discussions on the individual component in the cyclic model, including envelope curve, unloading curves, reloading curves, plastic strains and stress deterioration.

New equations were also developed based on the test results of FRP-confined ECC. Finally, cyclic models were proposed to predict the cyclic stress-strain behaviour of FRP-confined ECC. The predictions generated by the proposed models were compared with the corresponding test results. It is noted that the current study is focusing on the cyclic compressive behaviour and modelling of FRP-confined ECC. It is a continuous work of Li et al. [26], in which the monotonic compressive behaviour and modelling of FRP-confined ECC were presented by the authors. The proposed monotonic stress-strain model in Li et al. [26] is also adopted as the envelope model in the cyclic modelling in this study.

2. Test database for FRP-confined ECC

This section of the paper summarises the existing research on FRP-confined ECC. A test database was collected from five different sources as shown in Table 1. It consists of 86 specimens in total, in which 74 specimens were tested under monotonic compression and 12 specimens were tested under cyclic compression. All the specimens have the height-to-diameter of 2, with the diameter in the range of 100 - 500 mm. The unconfined ECC strength is in the range of 28.2 – 66.0 MPa and the confining materials vary from glass FRP (GFRP), carbon FRP (CFRP), polyethylene terephthalate FRP (PET FRP) to polyethylene naphthalate (PEN FRP). Dang et al. [21] experimentally investigated the compressive behaviour of FRP-confined ECC under monotonic and cyclic compressions. Through comparisons with FRP-confined normal concrete [41-43], failure mechanism was identified and design equations for ultimate conditions were proposed for FRP-confined ECC. Yuan et al. [23] noted that the lateral dilation of FRP-confined ECC could be further restrained to some extent because of the fibres in the ECC mixture. Existing dilation models [44,45] were found unable to provide accurate predictions and new axial strain-lateral strain model was developed based on the obtained test results. Li et al.[22] also investigated the monotonic and cyclic compressive behaviour of ECC cylinders confined by FRP tube and FRP jacket. An analysis-oriented model, which could predict the overall stress-strain behaviour, was proposed for monotonically loaded FRP-confined ECC. Yuan et al. [24] tested a series of FRP-confined ECC stub columns with different diameters and observed that with the increase of specimen size, ultimate strength would decrease while the corresponding ultimate axial strain would not be significantly affected. An equation of the ultimate compressive strength considering the size effect was proposed and was

found to outperform other existing models. Jiang et al. [25] investigated the monotonic compressive behaviour of PET FRP-confined ECC cylinders and noted that higher ductility could be achieved compared with conventional FRP-confined ECC. A load-path dependent analysis model was proposed, which incorporated the newly developed dilation model and actively-confined model as well as considering the stiffness change for the tensile behaviour of PET FRP.

It can be noted from the test database that both experimental investigations and modelling including design-oriented and analysis-oriented have been carried out for FRP-confined ECC, and most of the studies were focused on the monotonic compressive behaviour. Only Dang et al. [21] and Li et al. [22] conducted the cyclic compressive tests with 12 FRP-confined ECC specimens. Meanwhile, the modelling on FRP-confined ECC under cyclic compression is absent at the current stage. Therefore, this study focuses on the development of cyclic stress-strain model for FRP-confined ECC, which will contribute to the understanding of the behaviour of FRP-confined ECC under more comprehensive loading conditions. It is also worth noting that the test stress-strain curves included in Dang et al. [21] and Li et al. [22], which are two references providing the dataset for cyclically loaded FRP-confined ECC in this study, are with the ascending second-portion feature. It indicates that effective confinement has been achieved to generate the strain-hardening behaviour with enhanced compressive strength and strain for FRP-confined ECC. The cyclic model proposed in this study is also limited to this condition.

Table 1 Test database for FRP-confined ECC

Source	Number of specimens	Loading type	Specimen size (mm)	ECC strength f'_{c0} (MPa)	ECC strain ε_{c0}	FRP type	Confinement level $f_{lu,a}/f'_{c0}$	Strength enhancement ratio f'_{cu}/f'_{c0}	Strain enhancement ratio $\varepsilon_{cu}/\varepsilon_{c0}$
Dang et al. [21]	12	Monotonic & Cyclic	*D*=100; *H*=200	64.6-66.0	0.0035	CFRP	0.14 – 1.17	1.28 – 3.92	4.20 – 23.69
Li et al. [22]	18	Monotonic & Cyclic	*D*=100, 200; *H*=200, 400	40.0	0.0041	GFRP, CFRP	0.27 – 1.34	1.42 - 4.96	6.49 – 34.59
Yuan et al. [23]	15	Monotonic	*D*=150; *H*=300	28.2	0.0044	PEN FRP, PET FRP, GFRP	0.16 – 0.83	1.12 – 3.34	6.52 – 39.41
Yuan et al. [24]	32	Monotonic	*D*=100 - 500; *H*=200 - 1000	51.6	0.0027	PET FRP, GFRP	0.10 – 0.22	1.03 – 1.62	3.37 – 4.19
Jiang et al. [25]	9	Monotonic	*D*=100; *H*=200	35.2, 40.0	0.0026	PET FRP	N.A.	1.01 – 1.71	2.81 – 11.40
Total	86 specimens in total, in which 74 specimens for monotonic compression, 12 specimens for cyclic compression								

Notes: *D* and *H* are the nominal diameter and height of the specimens; f'_{c0} and ε_{c0} are the unconfined compressive strength and the corresponding strain of ECC; f'_{cu} and ε_{cu} are the ultimate compressive strength and ultimate axial strain at FRP rupture; $f_{lu,a}$ is the actual confinement pressure at FRP rupture with the expression of $f_{lu,a} = 2E_f t_f \varepsilon_{h,rup}/D$, in which E_f and t_f are the elastic modulus and thickness of confining FRP and $\varepsilon_{h,rup}$ is the actual hoop strain at FRP rupture.

3. Cyclic stress-strain model

3.1 Typical cyclic compressive behaviour and terminology

Fig. 1 presents the typical cyclic stress-strain curve for FRP-confined concrete, which encompasses the envelope curve, unloading curve and reloading curve. Envelope curve is the upper boundary of the unloading and reloading curves [30-32]. Point A on the envelope curve with the strain and stress of ε_{un} and σ_{un} is defined as the unloading point. Unloading curve starts from Point A with the stress reducing with the decrease of strain, and intersects with the horizontal axis at Point B. The strain ε_{pl} at Point B is named as plastic strain. Reloading curve initiates from Point B and stress increases with the increase of strain. Point C on the reloading curve is defined as the reference point, with the corresponding strain and stress of ε_{ref} and σ_{new}. Point C and Point A are at the same axial strain, which means ε_{ref} equals to ε_{un}. However, σ_{new} is lower than σ_{un}, which reflects the stress degradation during this loading cycle. Reloading curve intersects with the envelope curve at Point D with the strain and stress of $\varepsilon_{ret,env}$ and $\sigma_{ret,env}$. Then the loading process follows the envelope curve until the next unloading strain and starts the next loading cycle.

It is noted that the above definitions and the cyclic curve presented in Fig. 1 are corresponding to the case that the unloading point starts from the envelope curve, which is named as the envelope cycle. If the unloading point starts below the envelope curve, the cyclic curves are named as internal cycles [32]. In this study, both the test database and the investigated scope are related to the envelope cycles. Internal cycles and the corresponding model are not discussed in the current study.

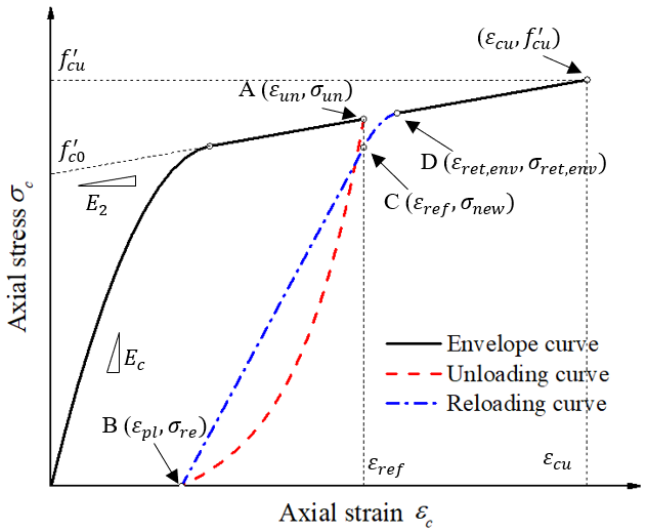

Fig. 1 Typical cyclic stress-strain model for FRP-confined concrete and key parameters

3.2 Envelope curve

Envelope curve is the upper boundary of cyclic stress-strain curve and is close to the stress-strain curve under monotonic compression for FRP-confined concrete [30-32]. Therefore, the envelope curve for cyclically loaded FRP-confined ECC can be generated with the stress-strain model for monotonically loaded FRP-confined ECC. Regarding the stress-strain models for confined concrete, Cavaleri et al. [46] reported that different models proposed by different researchers would have relatively large dispersion of the predicting results. Lam and Teng's design-oriented model [47] was developed for FRP-confined normal concrete and was widely adopted to predict the compressive behaviour of FRP-confined concrete under monotonic compression with good performance [48-52]. It consists of a first parabolic portion and a second linear portion, which is expressed as follows:

$$\sigma_c = \begin{cases} E_c\varepsilon_c - \frac{(E_c-E_2)^2}{4f'_{c0}}\varepsilon_c^2 & (0 \le \varepsilon_c \le \varepsilon_t) \\ f'_{c0} + E_2\varepsilon_c & (\varepsilon_t < \varepsilon_c \le \varepsilon_{cu}) \end{cases} \quad (1)$$

where f'_{c0} and E_c are unconfined compressive strength and elastic modulus of concrete. E_2 and ε_t are the slope of the second linear portion and the transition strain between the first parabolic portion and the second linear portion, with the following expressions:

$$E_2 = \frac{f'_{cu}-f'_{c0}}{\varepsilon_{cu}} \quad (2)$$

$$\varepsilon_t = \frac{2f'_{c0}}{E_c-E_2} \quad (3)$$

where f'_{cu} and ε_{cu} are the ultimate compressive strength and ultimate axial strain of confined concrete, which also directly affect the slope of the second linear portion of the stress-strain curve. In Li et al. [26], it was found that existing equations for the ultimate conditions developed for FRP-confined normal concrete could not perform well for the predictions for FRP-confined ECC. New equations were proposed to predict the ultimate compressive strength and ultimate axial strain according to the collected test data of FRP-confined ECC [26], with the expressions for f'_{cu} and ε_{cu} shown as follows:

$$\frac{f'_{cu}}{f'_{c0}} = 1 + 2.9(\rho_K - 0.01)(\rho_\varepsilon)^{0.9} \quad (4)$$

$$\frac{\varepsilon_{cu}}{\varepsilon_{c0}} = 1 + 21\rho_K^{0.98}\rho_\varepsilon^{1.02} \quad (5)$$

in which ε_{c0} is the compressive strain corresponding to f'_{c0} for unconfined ECC; ρ_K and ρ_ε are the confinement stiffness ratio and strain ratio with the following expressions:

$$\rho_K = \frac{K_l}{(f'_{c0}/\varepsilon_{c0})} = \frac{2E_f t_f}{(f'_{c0}/\varepsilon_{c0})D} \quad (6)$$

$$\rho_\varepsilon = \frac{\varepsilon_{h,rup}}{\varepsilon_{c0}} \quad (7)$$

in which D is the diameter of confined ECC; K_l is confining stiffness; E_f and t_f are the elastic modulus and thickness of confining FRP; $\varepsilon_{h,rup}$ is the FRP hoop rupture strain. Li et al. [26] modified the original Lam and Teng's model [47] with the proposed ultimate conditions as shown in Eqs. (4) and (5) and evaluated the applicability of the modified model for FRP-confined ECC. It was found that the predicted stress-strain curves are close to the test curves for FRP-confined ECC under monotonic compression. Two typical comparisons are presented in Fig. 2, while more comparisons can be referred to Li et al. [26]. Therefore, the modified Lam and Teng's model [26,47], with the expressions shown in Eqs. (1-7), is adopted to predict the envelope curve for FRP-confined ECC under cyclic compression.

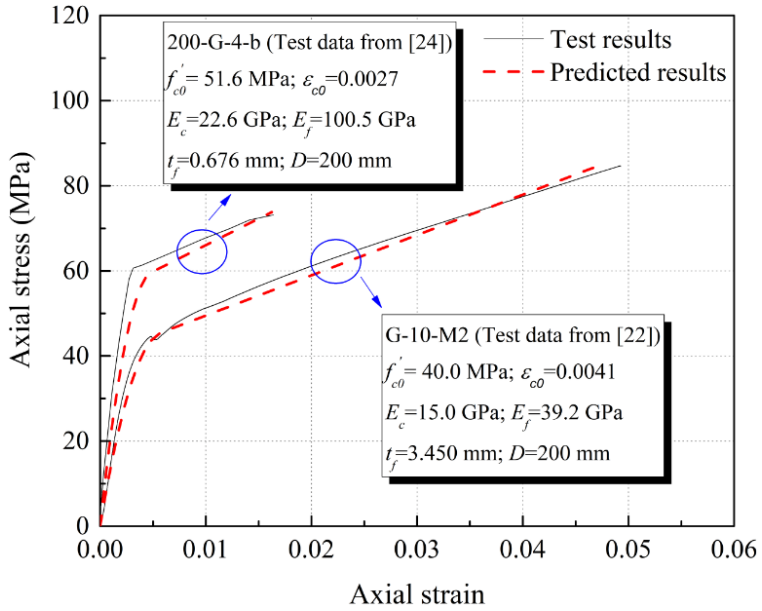

Fig. 2 Comparisons of monotonic stress-strain curves between test results and predicted results for FRP-confined ECC

3.3 Unloading paths

The FRP-confined ECC presents a similar unloading behaviour to that of FRP-confined normal concrete, which is a nearly linear portion at the initial stage, followed by an obviously nonlinear portion at the end stage. Typical existing unloading models developed for FRP-confined normal concrete [32-36], as shown in Table 2, were adopted to evaluate their performance on the prediction of unloading paths for FRP-confined ECC. Lam and Teng [32] and Yu et al. [33] adopted the same equation with polynomial form for the unloading path prediction. The coefficients and exponent are associated with the unloading strain ε_{un}, unloading stress σ_{un} and plastic strain ε_{pl}. Compared with Lam and Teng's model [32], Yu et al. [33] additionally considered the influence of concrete strength f'_{c0} on the exponent η for better prediction of the unloading behaviour of FRP-confined concrete with both normal strength and high strength. Wang et al. [34] and Hany et al. [35] used the same unloading equation, associated with unloading strain ε_{un}, unloading stress σ_{un} and plastic strain ε_{pl}. The curve shape is controlled by the two parameters B_0 and B_1, where B_0 is related to confining pressure f_l in Wang et al.'s model [34] whilst assigned as a constant in Hany et al.'s model [35], and B_1 is related to unloading strain ε_{un} in both two models. Except for the unloading strain ε_{un}, unloading stress σ_{un} and plastic strain ε_{pl}, Li et al. [36] also associated the unloading curve with confinement rigidity ρ, which is expressed as follows:

$$\rho = \frac{2E_f t_f}{D f'_{c0}} \tag{8}$$

Table 2 Existing cyclic stress-strain models developed for FRP-confined normal concrete

Objects	Lam and Teng [32]	Yu et al. [33]	Wang et al. [34]	Hany et al. [35]	Li et al. [36]
Unloading model	$\sigma_c = a\varepsilon_c^{\eta} + b\varepsilon_c + c$ $a = \frac{\sigma_{un} - E_{un,0}(\varepsilon_{un} - \varepsilon_{pl})}{\varepsilon_{un}^{\eta} - \varepsilon_{pl}^{\eta} - \eta\varepsilon_{pl}^{\eta-1}(\varepsilon_{un} - \varepsilon_{pl})}$ $b = E_{un,0} - \eta\varepsilon_{pl}^{\eta-1}a$ $c = -a\varepsilon_{pl}^{\eta} - b\varepsilon_{pl}$ $E_{un,0} = \min\left(\frac{0.5f'_{c0}}{\varepsilon_{un}}, \frac{\sigma_{un}}{\varepsilon_{un} - \varepsilon_{pl}}\right)$ $\eta = 350\varepsilon_{un} + 3$	Same as Lam and Teng [32] except for η $\eta = 40(350\varepsilon_{un} + 3)/f'_{c0}$	$\frac{\sigma_c}{\sigma_{un}} = B_0\left(\frac{\varepsilon_c - \varepsilon_{pl}}{\varepsilon_{un} - \varepsilon_{pl}}\right)^{B_1} + (1 - B_0)\left(\frac{\varepsilon_c - \varepsilon_{pl}}{\varepsilon_{un} - \varepsilon_{pl}}\right)$ $B_0 = 0.5 + 0.3\left(\frac{f_l}{f'_{c0}}\right)^{0.07} - 0.1\left(\frac{f_{ls}}{f'_{c0}}\right)^{0.04}$ for $\varepsilon_{un} \le 0.02$, $B_1 = -0.02\left(\frac{\varepsilon_{un}}{\varepsilon_{c0}}\right)^2 + 0.46\left(\frac{\varepsilon_{un}}{\varepsilon_{c0}}\right) + 1.76$ for $\varepsilon_{un} > 0.02$, $B_1 = 4.36$	$\frac{\sigma_c}{\sigma_{un}} = B_0\left(\frac{\varepsilon_c - \varepsilon_{pl}}{\varepsilon_{un} - \varepsilon_{pl}}\right)^{B_1} + (1 - B_0)\left(\frac{\varepsilon_c - \varepsilon_{pl}}{\varepsilon_{un} - \varepsilon_{pl}}\right)$ $B_0 = 0.8$ $B_1 = 2.172\left(\frac{\varepsilon_{un}}{\varepsilon_{c0}}\right)^{0.324}$	$\sigma_c = E_{un,0}\left(\frac{\varepsilon_c}{\varepsilon_{pl}}\right)^m (\varepsilon_c - \varepsilon_{pl})$ $\frac{E_{un,0}}{E_c} = 0.21\left(\frac{f'_{c0}}{f'_{30}}\right)^{0.195}\rho^{-0.031}\left(\frac{\varepsilon_{un}}{\varepsilon_{c0}}\right)^{-1.115}$ $m = \log_{\left(\frac{\varepsilon_{un}}{\varepsilon_{pl}}\right)}\left(\frac{\sigma_{un}}{E_{un,0}(\varepsilon_{un} - \varepsilon_{pl})}\right)$
Plastic strain	for $0 < \varepsilon_{un} \le 0.001$, $\varepsilon_{pl} = 0$ for $0.001 < \varepsilon_{un} < 0.0035$, $\varepsilon_{pl} = [1.4(0.87 - 0.004f'_{c0}) - 0.64](\varepsilon_{un} - 0.001)$ for $0.0035 \le \varepsilon_{un} \le \varepsilon_{cu}$, $\varepsilon_{pl} = (0.87 - 0.004f'_{c0})\varepsilon_{un} - 0.0016$	for $0 < \varepsilon_{un} \le 0.001$, $\varepsilon_{pl} = 0$ for $0.001 < \varepsilon_{un} \le 0.0035$, $\varepsilon_{pl} = 0.184\varepsilon_{un} - 0.0002$ for $0.0035 < \varepsilon_{un} \le \varepsilon_{cu}$, $\varepsilon_{pl} = 0.703\varepsilon_{un} - 0.002$	for $0 < \varepsilon_{un} \le 0.001$, $\varepsilon_{pl} = 0$ for $0.001 < \varepsilon_{un} \le 0.004$, $\varepsilon_{pl} = 0.42\varepsilon_{un} - 0.0004$ for $0.004 < \varepsilon_{un} \le \varepsilon_{cu}$, $\varepsilon_{pl} = 0.815\varepsilon_{un} - 0.002$	for $0 < \varepsilon_{un} \le 0.001$, $\varepsilon_{pl} = 0$ for $0.001 < \varepsilon_{un} \le 0.0035$, $\varepsilon_{pl} = 0.4552\varepsilon_{un} - 0.0003$ for $0.0035 < \varepsilon_{un} \le \varepsilon_{cu}$, $\varepsilon_{pl} = 0.7827\varepsilon_{un} - 0.0014$	for $0 < \varepsilon_{un} \le 0.001$, $\varepsilon_{pl} = 0$ for $0.001 < \varepsilon_{un} \le \varepsilon_{cu}$, $\varepsilon_{pl} = 0.353\left(\frac{f'_{c0}}{f'_{30}}\right)^{-0.4}(\varepsilon_{un} - 0.001) + 3.36\rho^{-0.178}(\varepsilon_{un} - 0.001)^{1.414}$
Stress deterioration	for $0 < \varepsilon_{un} \le 0.001$, $\varphi = 1$ for $0.001 < \varepsilon_{un} < 0.002$, $\varphi = 1 - 80(\varepsilon_{un} - 0.001)$ for $0.002 \le \varepsilon_{un} \le \varepsilon_{cu}$, $\varphi = 0.92$	for $0 < \varepsilon_{un} \le 0.001$, $\varphi = 1$ for $0.001 < \varepsilon_{un} \le 0.0035$, $\varphi = 1 - 32(\varepsilon_{un} - 0.001)$ for $0.0035 < \varepsilon_{un} \le \varepsilon_{cu}$, $\varphi = 0.92$	$\varphi = 0.912$	for $0 < \varepsilon_{un} \le 0.001$, $\varphi = 1$ for $0.001 < \varepsilon_{un} \le \varepsilon_{cu}$, $\varphi = 0.938$	N.A.
Reloading model	for $\varepsilon_{re} \le \varepsilon_c \le \varepsilon_{ref}$, $\sigma_c = \sigma_{re} + E_{re}(\varepsilon_c - \varepsilon_{re})$ for $\varepsilon_{ref} \le \varepsilon_c \le \varepsilon_{ret,env}$, $\sigma_c = A{\varepsilon_c}^2 + B\varepsilon_c + C$ $E_{re} = (\sigma_{new} - \sigma_{re})/(\varepsilon_{ref} - \varepsilon_{re})$ $\sigma_{new} = \varphi\sigma_{un}$ $B = E_{re} - 2A\varepsilon_{ref}$ $C = \sigma_{new} - A{\varepsilon_{ref}}^2 - B\varepsilon_{ref}$ for $\varepsilon_{ret,env} < \varepsilon_t$, $A = \frac{(E_C - E_2)^2(E_{re}\varepsilon_{ref} - \sigma_{new}) + (E_C - E_{re})^2 f'_{c0}}{4(\sigma_{new} - E_c\varepsilon_{ref})f'_{c0} + (E_C - E_2)^2{\varepsilon_{ref}}^2}$ $\varepsilon_{ret,env} = \frac{E_c - B}{2A + \frac{(E_C - E_2)^2}{f'_{c0}}}$ for $\varepsilon_{ret,env} \ge \varepsilon_t$, $A = \frac{(E_{re} - E_2)^2}{4(\sigma_{new} - f'_{co} - E_2\varepsilon_{ref})}$ $\varepsilon_{ret,env} = \frac{E_2 - B}{2A}$	Same as Lam and Teng [32]	$\sigma_c = E_{re}(\varepsilon_c - \varepsilon_{pl})$ $E_{re} = \frac{\sigma_{new}}{\varepsilon_{un} - \varepsilon_{pl}}$ $\sigma_{new} = \varphi\sigma_{un}$	$\sigma_c = E_{re}(\varepsilon_c - \varepsilon_{pl})$ $E_{re} = \frac{\sigma_{new}}{\varepsilon_{un} - \varepsilon_{pl}}$ $\sigma_{new} = \varphi\sigma_{un}$	$\sigma_c = \frac{(E_{re} - E_2)(\varepsilon_c - \varepsilon_{pl})}{\left(1 + \left(\frac{(E_{re} - E_2)(\varepsilon_c - \varepsilon_{pl})}{f_r}\right)^n\right)^{1/n}} + E_2(\varepsilon_c - \varepsilon_{pl})$ $\frac{E_{re}}{E_c} = \left(\frac{f'_{c0}}{f'_{30}}\right)^{0.032}\bar{\varepsilon}^{-0.409} - 0.317\rho^{-0.064\bar{\varepsilon}}$ for $E_2 \ge 0$, $\frac{f_r}{f'_{c0}} = 0.693\frac{\sigma_{un}}{f'_{c0}} + 0.337\rho^{-0.053}$ for $E_2 < 0$, $\frac{f_r}{f'_{c0}} = 0.969\frac{\sigma_{un}}{f'_{c0}} + 1.981\rho^{-2.012}$ $\bar{\varepsilon} = \varepsilon_{un}/\varepsilon_{c0} \le 10$ $n = 2.61\left(\frac{\varepsilon_{un}}{\varepsilon_{c0}}\right) + 4.88$

Predictions of unloading paths for FRP-confined ECC with the five unloading models are presented in Fig. 3 with the comparisons to test results. It can be noted that the predictions by different models are close to each other and test results for the unloading paths with low unloading strains. Relatively larger deviations can be noted for the unloading paths with larger unloading strains. Lam and Teng's model [32] and Yu et al.'s model [33] provide lower stress predictions for the nonlinear portion at the end stage in each unloading path. In general, Wang et al.'s model [34] can generate the closest unloading curves compared with test curves, which indicates that it is applicable to the prediction of unloading behaviour of FRP-confined ECC. It should be noted that for the evaluation of the five existing unloading models as presented in Fig. 3, actual unloading strain ε_{un}, unloading stress σ_{un} and plastic strain ε_{pl} were used to ensure that the prediction accuracy was dependent on the unloading model only, excluding the influence of unloading stress σ_{un} and plastic strain ε_{pl}. This evaluation method has also been adopted in the literature [14,37].

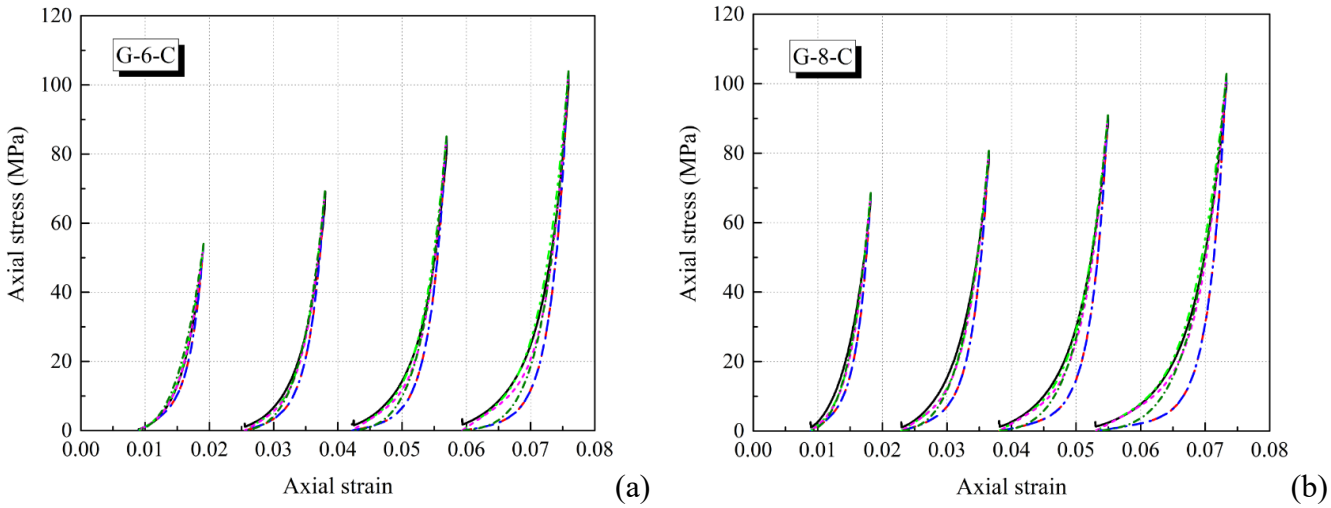

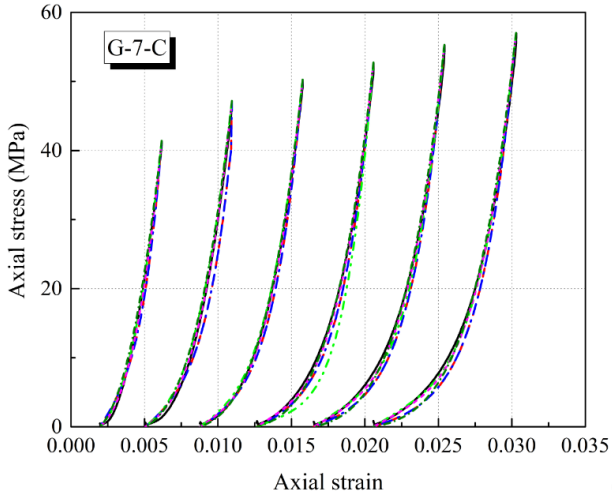
G-7-C
Axial stress (MPa)
Axial strain
0
20
40
60
0.000
0.005
0.010
0.015
0.020
0.025
0.030
0.035

(c)

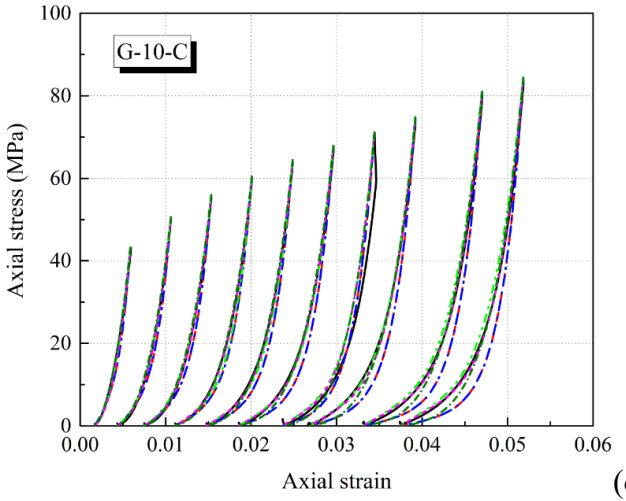
G-10-C
Axial stress (MPa)
Axial strain
0
20
40
60
80
100
0.00
0.01
0.02
0.03
0.04
0.05
0.06

(d)

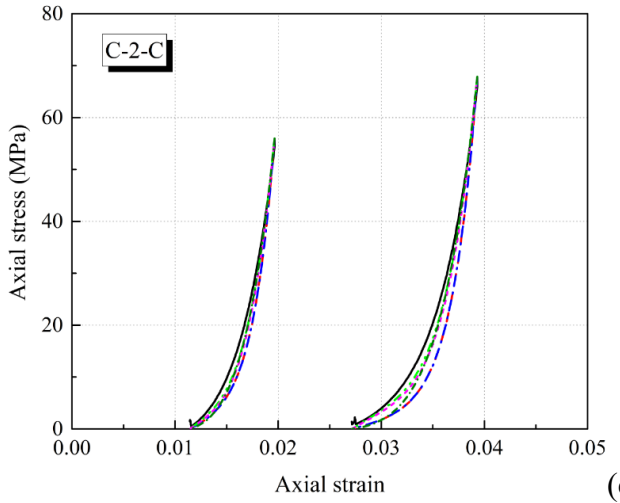
C-2-C
Axial stress (MPa)
Axial strain
0
20
40
60
80
0.00
0.01
0.02
0.03
0.04
0.05

(e)

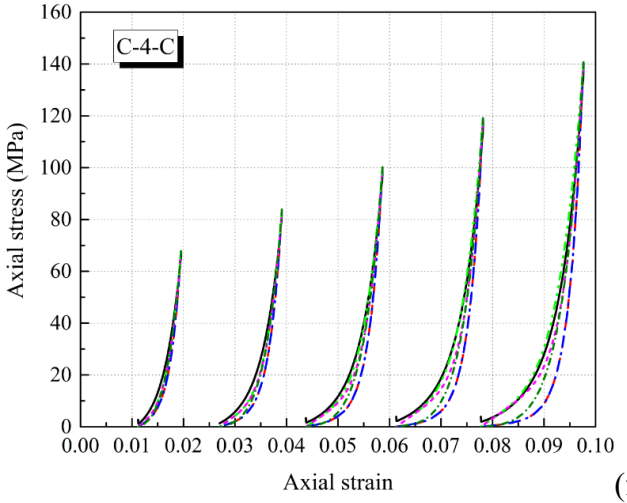
C-4-C
Axial stress (MPa)
Axial strain
0
20
40
60
80
100
120
140
160
0.00
0.01
0.02
0.03
0.04
0.05
0.06
0.07
0.08
0.09
0.10

(f)

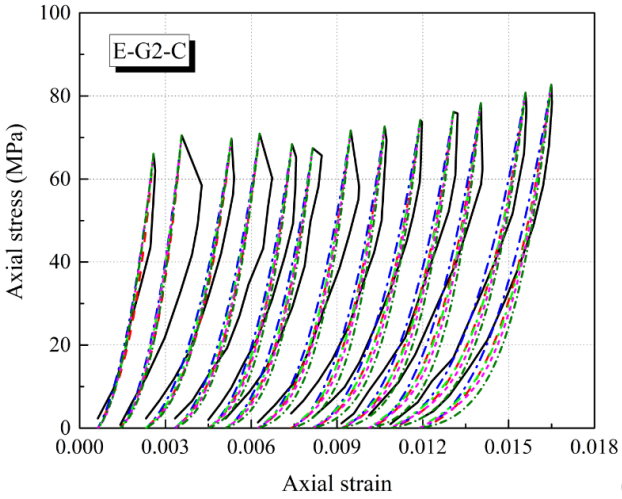
E-G2-C
Axial stress (MPa)
Axial strain
0
20
40
60
80
100
0.000
0.003
0.006
0.009
0.012
0.015
0.018

(g)

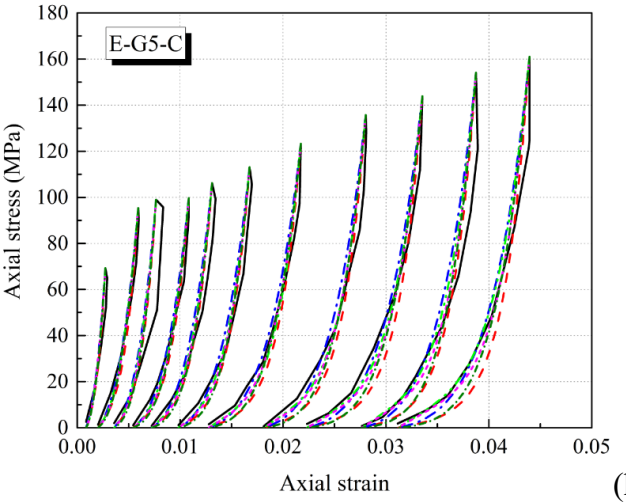
E-G5-C
Axial stress (MPa)
Axial strain
0
20
40
60
80
100
120
140
160
180
0.00
0.01
0.02
0.03
0.04
0.05

(h)

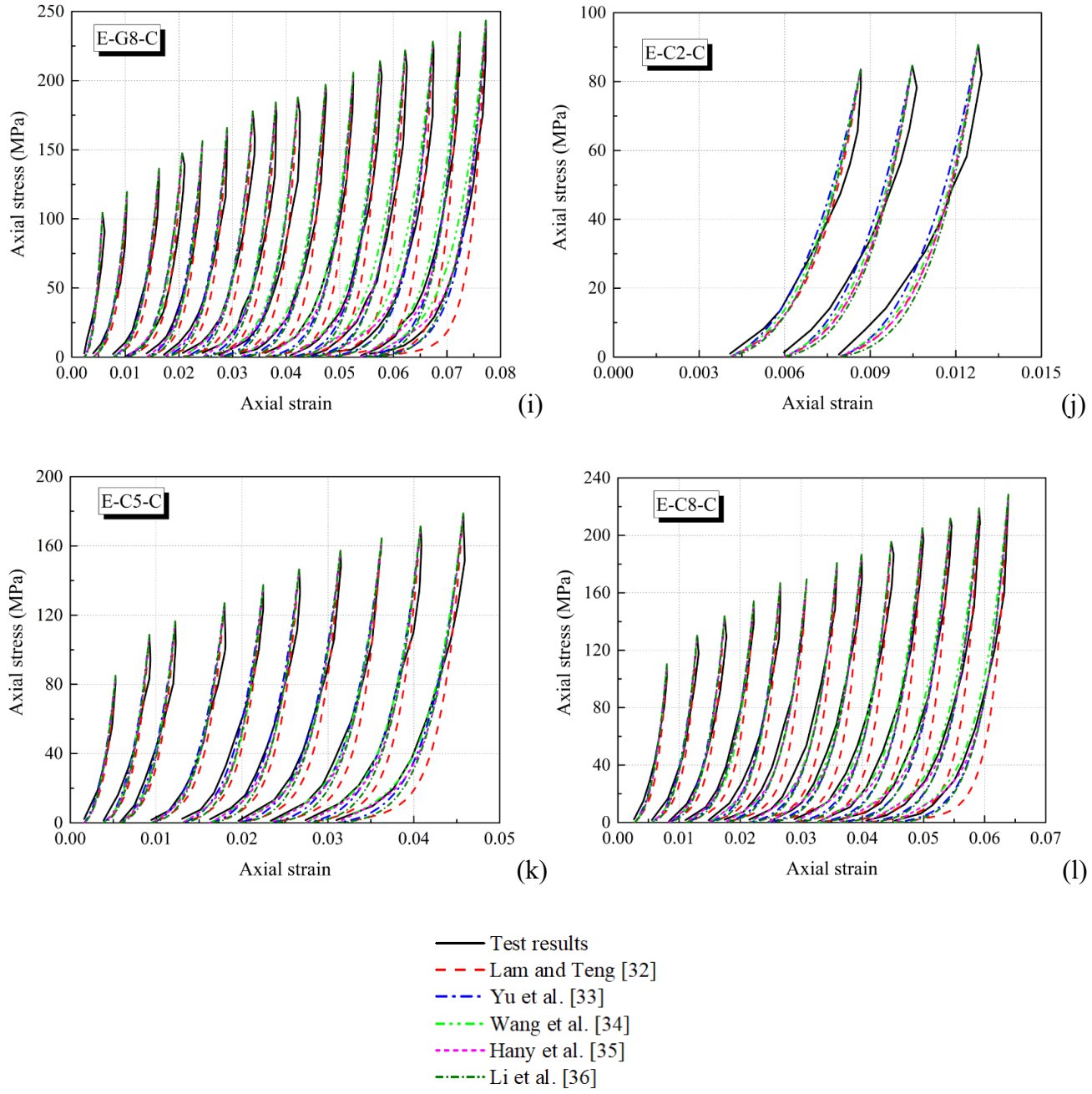

Fig. 3 Evaluation of different unloading models

3.4 Plastic strains

Plastic strain is a key parameter controlling the shape of the unloading path. It equals to the axial strain at the intersection point between the unloading curve and the zero-horizontal axis. Typical prediction equations of plastic strain developed for FRP-confined normal concrete are summarised in Table 2. They all adopt the linear relationship between plastic strain and unloading strain, except that Lam and Teng's model [32] and Li et al.'s model [36] additionally consider the effect of concrete strength. Meanwhile, Li et al.'s model [36] also takes the confinement rigidity into account like its unloading model. Test results of plastic strain, together

with the corresponding unloading strains, were extracted from the test cyclic stress-strain curves for FRP-confined ECC. As plotted in Fig. 4, plastic strain is basically increasing linearly with the increase of unloading strain, which is similar to the behaviour of FRP-confined normal concrete, though slightly nonlinear behaviour at larger unloading strains can be observed. In Table 3, it summarises the linear equations between plastic strain and unloading strain ($\varepsilon_{pl} = a\varepsilon_{un} + b$) for all the twelve available cyclic specimens in the literature [21,22], according to the regression analysis with the corresponding test data. The coefficients of determination (R^2) are all close to 1, demonstrating the good behaviour of the linear regression. Fig. 5 plots the parameters a and b for specimens with different ECC compressive strengths and FRP confinement rigidities. It can be seen that parameter a is independent of ECC strength and confinement rigidity [as shown in Figs. 5(a-b)] and it is also challenging to identify the effect of ECC strength on the value of parameter b [as shown in Figs. 5(c)]. However, relatively obvious descending tendency of parameter b can be noted with the increase of confinement rigidity [as shown in Figs. 5(d)]. Therefore, it can be regarded that for FRP-confined ECC under cyclic compression, if linear relationship between plastic strain and unloading strain is considered, the linear relationship is not associated with ECC compressive strength. For confinement rigidity, it does not affect the slope (parameter a) while has influence on the intercept (parameter b).

Table 3 Linear relations between unloading strains and plastic strains for specimens under cyclic compression

Source	Specimen ID	$\varepsilon_{pl} = a\varepsilon_{un} + b$		R^2
		a	b	
Li et al. [22]	G-6-C	0.8855	-0.0080	0.9999
	G-8-C	0.8030	-0.0060	0.9998
	G-7-C	0.7780	-0.0032	0.9986
	G-10-C	0.7914	-0.0042	0.9972
	C-2-C	0.7987	-0.0043	1.0000
	C-4-C	0.8573	-0.0061	0.9997
Dang et al. [21]	E-G2-C	0.8211	-0.0016	0.9972
	E-G5-C	0.7509	-0.0024	0.9957
	E-G8-C	0.7799	-0.0047	0.9964
	E-C2-C	0.9206	-0.0038	0.9961
	E-C5-C	0.7344	-0.0031	0.9977
	E-C8-C	0.7650	-0.0051	0.9960

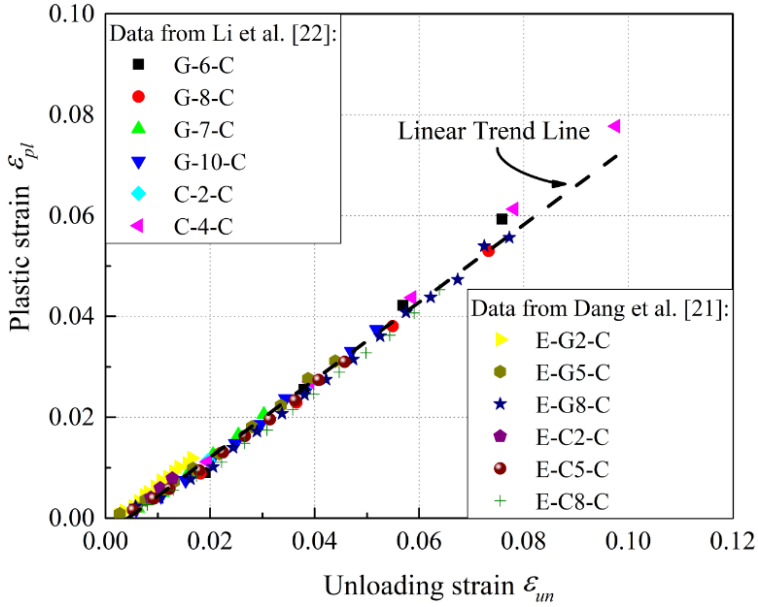

Fig. 4 Relationship between plastic strain and unloading strain

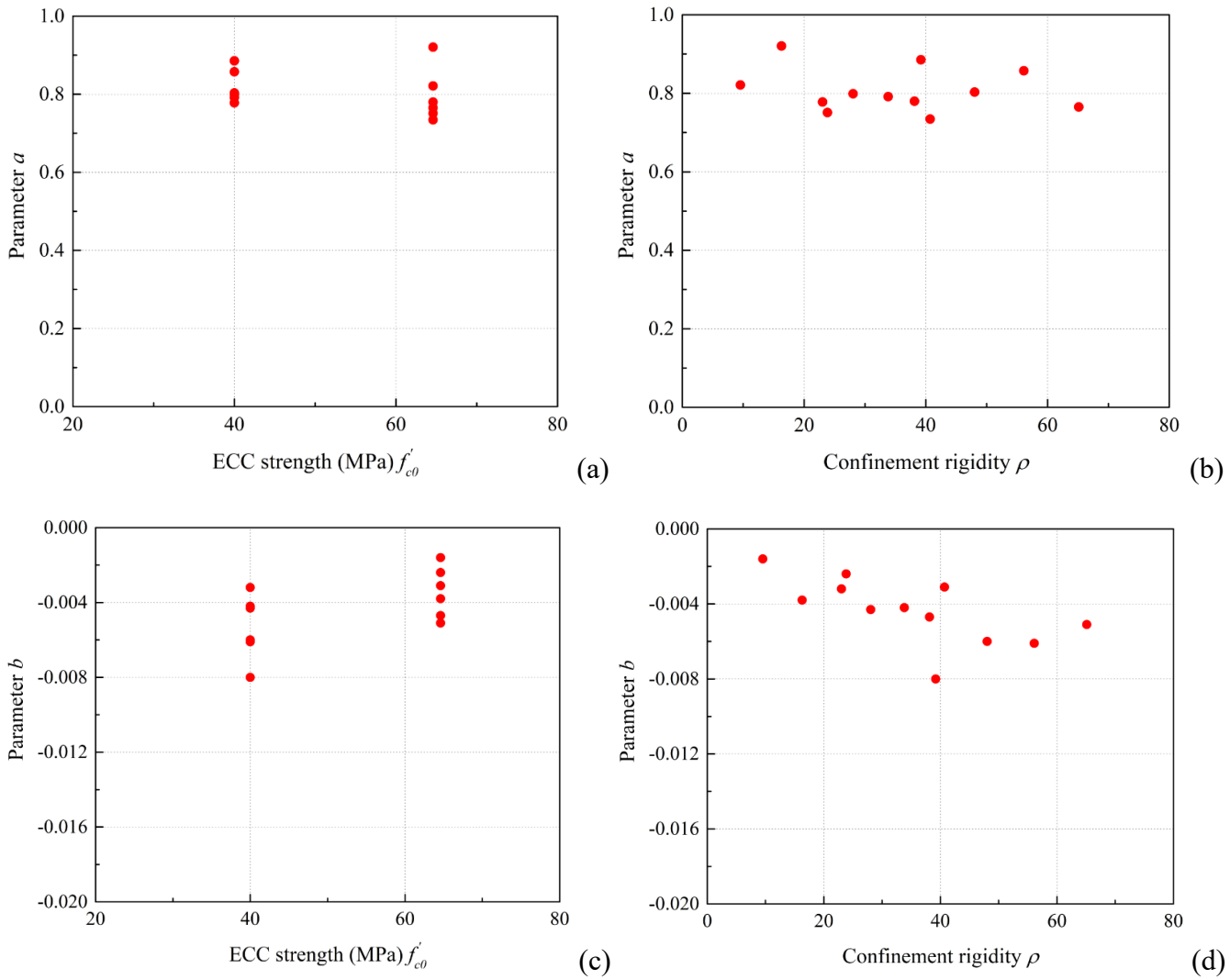

Fig. 5 Parameters a and b with different ECC compressive strengths and FRP confinement rigidities

The existing prediction models are evaluated as shown in Figs. 6(a-e). It can be observed that compared with the test results, Lam and Teng's model [32] and Yu et al.'s model [33] provide lower predictions, while Wang et al.'s model [34], Hany et al.'s model [35] and Li et al.'s model [36] generate higher predictions. It reveals that these plastic strain models developed for FRP-confined normal concrete cannot provide accurate predictions for FRP-confined ECC. Based on the observation obtained from Fig. 5, new linear equation is proposed as follows, in which the intersect (parameter b in $\varepsilon_{pl} = a\varepsilon_{un} + b$) is associated with confinement rigidity ρ:

$$\varepsilon_{pl} = \begin{cases} 0, & 0 < \varepsilon_{un} \leq 0.002 \\ 0.6032\varepsilon_{un} - 0.0011, & 0.002 < \varepsilon_{un} \leq 0.009 \\ 0.8067\varepsilon_{un} - (0.00008\rho + 0.0016), & 0.009 < \varepsilon_{un} \leq \varepsilon_{cu} \end{cases} \quad (9)$$

For the plastic strain models presented in Table 2, $\varepsilon_{pl} = 0$ is considered for $\varepsilon_{un} \leq 0.001$. For the models proposed by Lam and Teng [32], Yu et al. [33], Wang et al. [34] and Hany et al. [35], a different linear equation is considered in the lower unloading strain range of $0.001 < \varepsilon_{un} \leq 0.0035\ or\ 0.004$, compared with that in the higher unloading range of $0.0035\ or\ 0.004 < \varepsilon_{un} \leq \varepsilon_{cu}$. These piecewise functions aim to generate close predictions of plastic strains at both lower and higher unloading strains. It should be noted that unloading strains in the range of $0.001 < \varepsilon_{un} \leq 0.0035\ or\ 0.004$ are quite low, while most of the test data fall in the range of $0.0035\ or\ 0.004 < \varepsilon_{un} \leq \varepsilon_{cu}$ for cyclically loaded FRP-confined normal concrete. For FRP-confined ECC in this study, the similar consideration is adopted. In the current database, all plastic strains are larger than 0.002, leading to the assumption of $\varepsilon_{pl} = 0$ when $\varepsilon_{un} \leq 0.002$ in Eq. (9). With regression analysis, meanwhile, a larger unloading strain value 0.009 is assigned to the dividing point of the piecewise function as shown in Eq. (9). Performance of Eq. (9) is presented in Fig. 6(f), in which close predictions on plastic strains are obtained compared with test results.

It is worth noting that the above analysis and proposed Eq. (9) are based on the assumption of linear relationship between plastic strain and unloading strain. As observed in Fig. 4, nonlinear relationship with power function can be adopted as well to describe the slightly nonlinear behaviour between plastic strain and unloading strain at larger unloading strains. The following equation is proposed through regression analysis:

$$\varepsilon_{pl} = \begin{cases} 0, & 0 < \varepsilon_{un} \leq 0.002 \\ 1.255(\varepsilon_{un})^{1.2}, & 0.002 < \varepsilon_{un} \leq \varepsilon_{cu} \end{cases} \quad (10)$$

Fig. 6(g) presents the comparison between test results and predicted results. The close agreement shows the good performance of the proposed equation as shown in Eq. (10). Compared with linear equations, the proposed power function Eq. (10) can cater the prediction of plastic strains at both lower and higher unloading strains in the range of $0.002 < \varepsilon_{un} \leq \varepsilon_{cu}$ with one equation in a simpler manner. It is not associated with ECC strength and confinement rigidity.

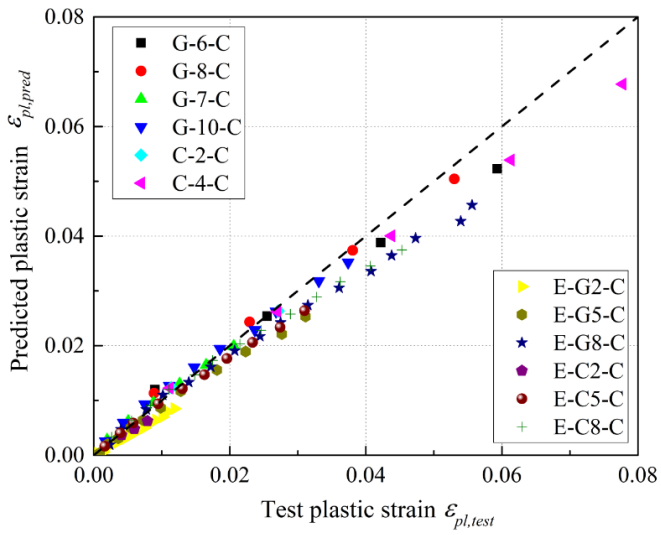

(a) Lam and Teng' s model [32]

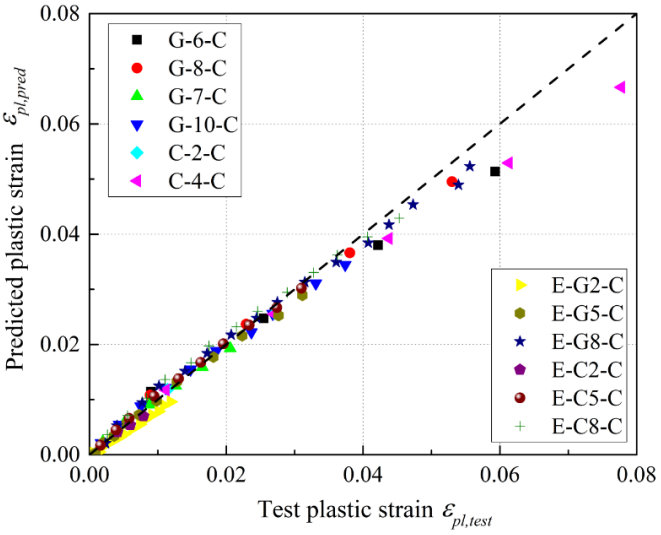

(b) Yu et al.'s model [33]

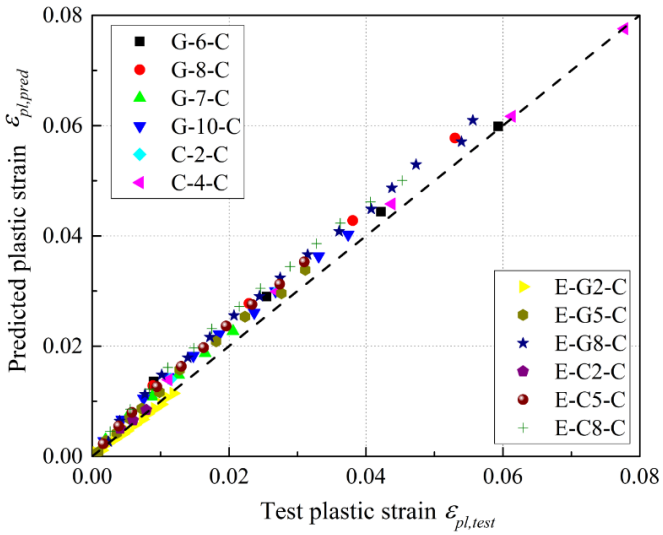

(c) Wang et al.' s model [34]

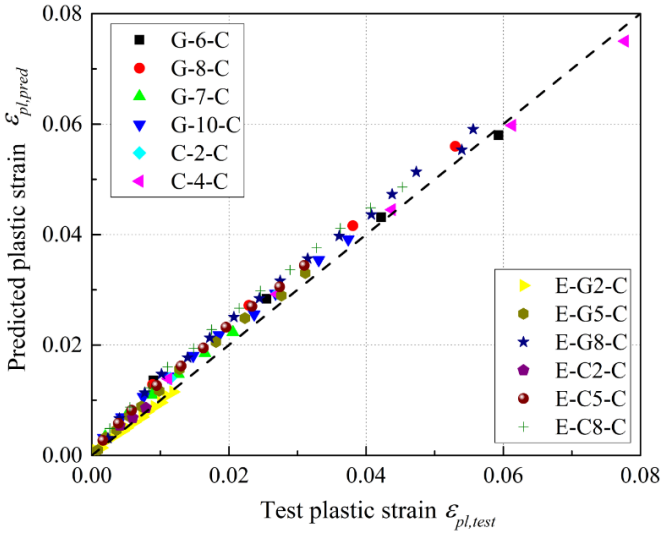

(d) Hany et al.'s model [35]

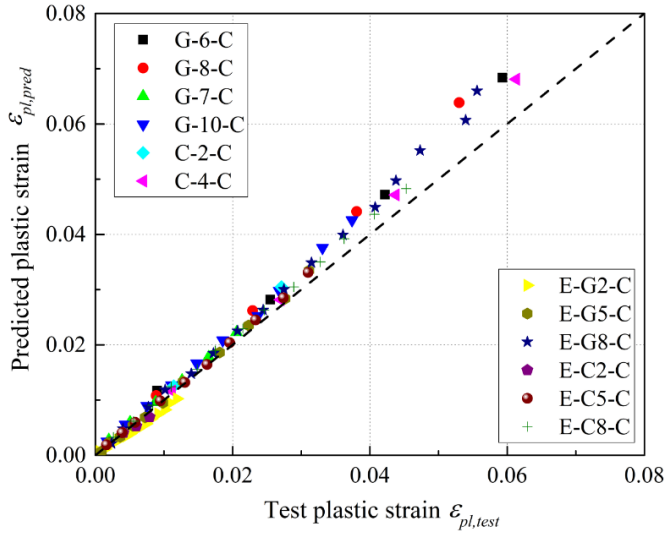

(e) Li et al.' s model [36]

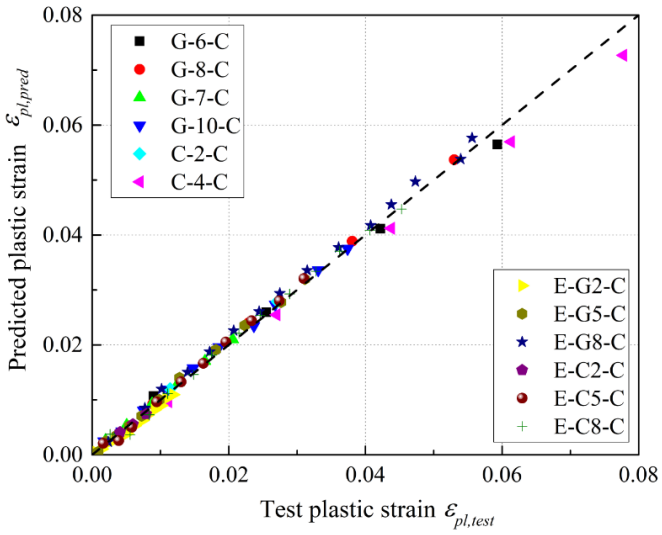

(f) Proposed Eq. (9)

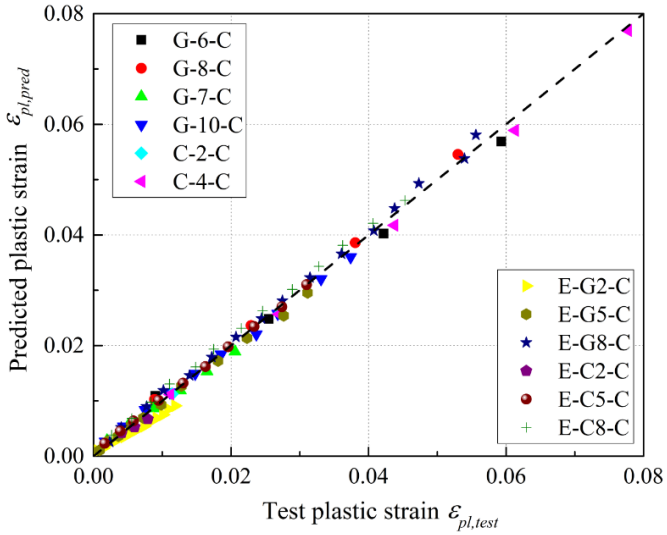

(g) Proposed Eq. (10)

Fig. 6 Evaluation of different plastic strain models

Statistical indicators including mean (M), coefficient of variation (COV), average absolute error (AAE) and coefficient of determination (R^2) were also used to evaluate the accuracy of the predictions by the proposed models and the other existing models, with the expressions given in the following Eqs. (11-14):

$$M = \frac{1}{n}\sum_{i=1}^{n}\frac{y_{test,i}}{y_{pred,i}} \tag{11}$$

$$COV = \frac{1}{M}\sqrt{\frac{\sum_{i=1}^{n}(\frac{y_{test,i}}{y_{pred,i}}-M)^2}{n-1}} \quad (12)$$

$$AAE = \frac{1}{n}\sum_{i=1}^{n}\left|\frac{y_{test,i}-y_{pred,i}}{y_{test,i}}\right| \quad (13)$$

$$R^2 = 1 - \frac{\sum_{i=1}^{n}(y_{test,i}-y_{pred,i})^2}{\sum_{i=1}^{n}(y_{test,i}-\frac{1}{n}\sum_{i=1}^{n}y_{test,i})^2} \quad (14)$$

in which $y_{test,i}$ and $y_{pred,i}$ are the i^{th} test result and model predicted result, n is the total number of the test plastic strains collected from the cyclic stress-strain curves. Statistical performance of different plastic strain models is presented in Fig. 7. Compared with the existing models [32-36] developed for FRP-confined normal concrete, the newly proposed models [Eqs. (9) and (10)] developed based on the database of FRP-confined ECC have more outstanding performance. Eq. (9) provides predictions with M, COV, AAE and R^2 of 1.019, 0.146, 0.106 and 0.994, and Eq. (10) provides predictions with M, COV, AAE and R^2 of 0.994, 0.146, 0.105 and 0.994, respectively. Compared to Eq. (9) with linear function form, Eq. (10) with power function form is using simpler expression and can generate slightly better predictions with mean value closer to 1. Meanwhile, the linear tendency between plastic strain and unloading strain decreases at high unloading strains as shown in Fig. 4. Power function form is also more logic to describe this nonlinear behaviour. Therefore, Eq. (10) is used to predict the plastic strain in the development of cyclic model for FRP-confined ECC in this study.

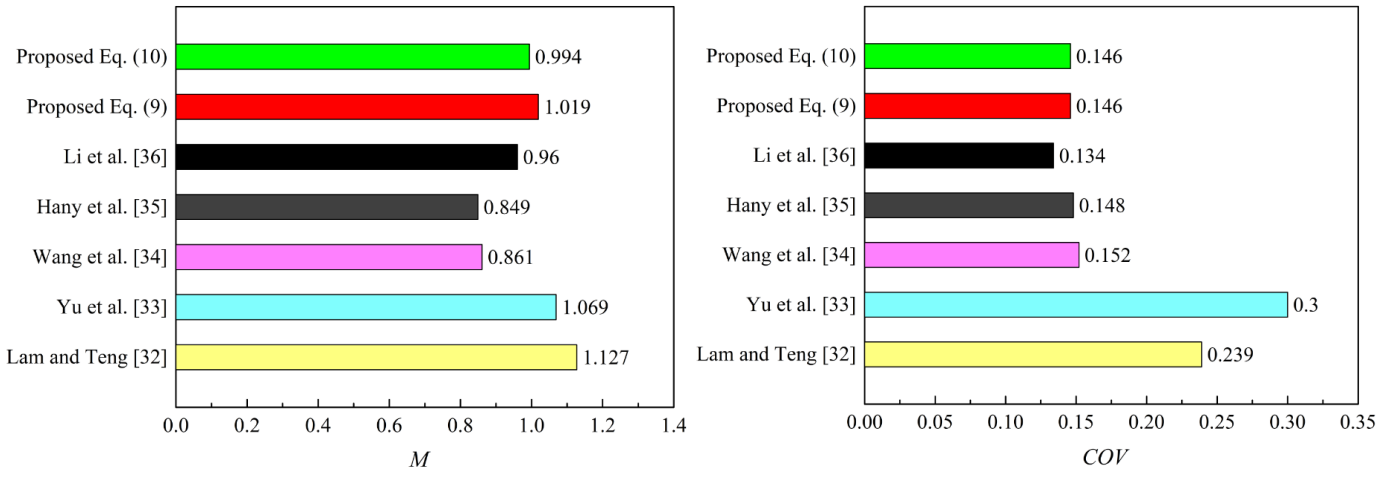

(a) Mean (b) Coefficient of variation

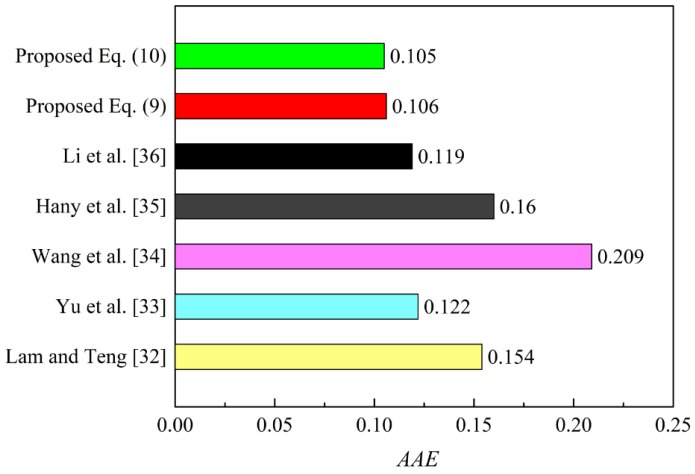

(c) Average absolute error

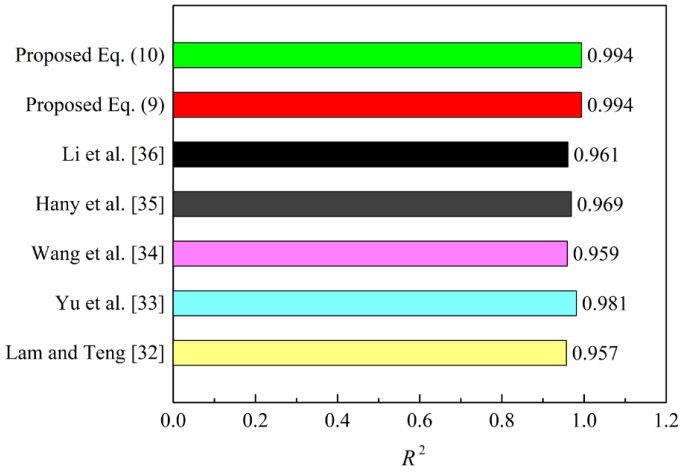

(d) Coefficient of determination

Fig. 7 Statistical performance of different plastic strain models

3.5 Stress deterioration

Stress deterioration φ is a parameter used to depict the degradation behaviour of FRP-confined concrete under cyclic loadings. It can be expressed as follows:

$$\varphi = \frac{\sigma_{new}}{\sigma_{un}} \tag{15}$$

where σ_{un} is the unloading stress and σ_{new} is the stress in the reloading curve at the reference strain ε_{ref}, which also equals to the unloading strain ε_{un} as shown in Fig. 1. In Table 2, it summarises that the expression of stress deterioration φ is in the range of 0.912 – 1.0 for the typical models developed for FRP-confined normal concrete [32-36]. In the current study, the values of stress deterioration φ at different unloading strains were calculated following the definition presented in Eq. (15) based on the available test data of cyclically loaded FRP-confined ECC and are plotted in Fig. 8. In the current database, all the unloading strains are larger than 0.002. In this range, the stress deterioration can be considered independent of the unloading strain as shown in Fig. 8, which is a similar behaviour to FRP-confined normal concrete. The average value of $\varphi = 0.936$ was obtained by regression analysis using the test data for the range of unloading strain $0.002 < \varepsilon_{un} \leq \varepsilon_{cu}$. Similar to Lam and Teng's model [32] and Yu et al.'s model [33] as presented in Table 2, φ is assigned to be 1.0 for $0 < \varepsilon_{un} \leq 0.001$ and linear relationship between φ and ε_{un} is adopted for $0.001 < \varepsilon_{un} \leq 0.002$.

Therefore, the equation of stress deterioration is expressed in Eq. (16) and also adopted in the prediction model of cyclic stress-strain curve for FRP-confined ECC.

$$\varphi = \begin{cases} 1, & 0 < \varepsilon_{un} \le 0.001 \\ 1 - 64(\varepsilon_{un} - 0.001), & 0.001 < \varepsilon_{un} \le 0.002 \\ 0.936, & 0.002 < \varepsilon_{un} \le \varepsilon_{cu} \end{cases} \quad (16)$$

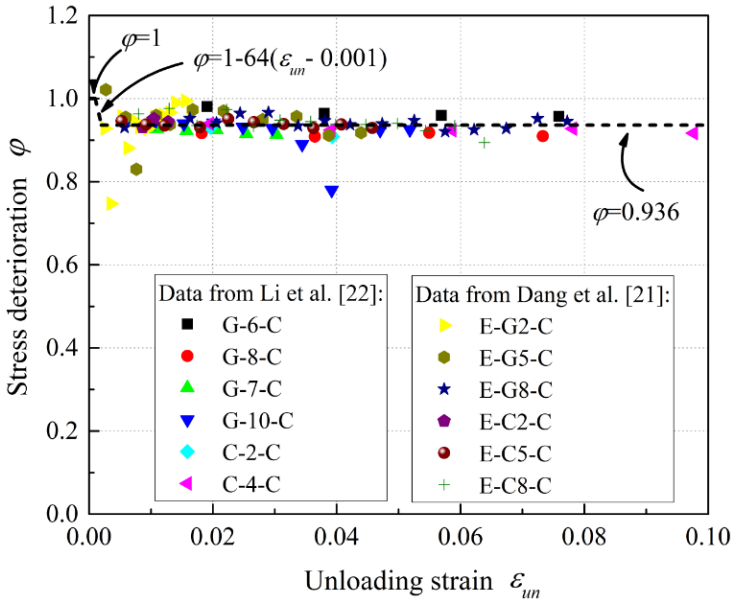

Fig. 8 Stress deteriorations at different unloading strains

3.6 Reloading paths

For the typical reloading path of FRP-confined concrete as shown in Fig. 1, it is featured with a linear portion starting from the plastic strain point $(\varepsilon_{pl}, 0)$ followed by a nonlinear portion intersecting with the envelope curve. Smooth transition is ensured between the two portions. In Table 2, it summarises the five existing reloading models developed for FRP-confined normal concrete. Lam and Teng 's model [32] and Yu et al.'s model [33] adopt the same equation form, which is using a linear curve from the plastic strain point $(\varepsilon_{pl}, 0)$ to the reference point $(\varepsilon_{ref}, \sigma_{new})$ and a parabolic curve afterwards until the reloading curve intersects with the envelope curve. Wang et al.'s model [34] and Hany et al.'s model [35] simply neglect the nonlinear behaviour of the reloading path and directly adopt the linear curve from the plastic strain point $(\varepsilon_{pl}, 0)$ to the envelope curve, which passes through the reference point $(\varepsilon_{ref}, \sigma_{new})$. Li et al.'s model [36] adopts the function characterising by two approximately linear curves and a nonlinear transition curve in between. In this

study, since Wang et al.'s model [34] and Hany et al.'s model [35] cannot capture the nonlinear reloading behaviour, only Lam and Teng 's model [32], Yu et al.'s model [33] and Li et al.'s model [36] were used to evaluate the applicability for the reloading path prediction of FRP-confined ECC.

4. Proposed cyclic stress-strain models and validation

In Section 3 of this paper, different components of cyclic stress-strain model for FRP-confined ECC, including envelope curve, unloading and reloading paths, plastic strain as well as stress deterioration, have been discussed in detail. Lam and Teng's model [47] was modified with the new equations of ultimate compressive strength and ultimate axial strain [26]. It could provide close predictions of the stress-strain curve for FRP-confined ECC under monotonic compression, which is also regarded as the envelope curve of FRP-confined ECC under cyclic compression. Five typical unloading models were evaluated and Wang et al.'s unloading model [34] was found to generate the closest predictions for FRP-confined ECC. Based on the available test data, new equations for predicting the plastic strain [as shown in Eq. (10)] and stress deterioration [as shown in Eq. (16)] were proposed for FRP-confined ECC. Meanwhile, Lam and Teng's model [32] and Li et al.'s model [36] were selected to capture the characteristics of the reloading behaviour of FRP-confined ECC. With these determined components, cyclic stress-strain model of FRP-confined ECC can be developed.

Fig. 9 shows the comparison between the predicted curves and test curves for cyclically loaded FRP-confined ECC. Model I consists of the modified Lam and Teng's enveloped model [26,47], Wang et al.'s unloading model [34], newly proposed plastic strain model and stress deterioration model [Eqs. (10) and (16)] as well as Lam and Teng's reloading model [32]; while Model II consists of the modified Lam and Teng's enveloped model [26,47], Wang et al.'s unloading model [34], newly proposed plastic strain model [Eq. (10)] as well as Li et al.'s reloading model [36], as shown in Fig. 10. For the predicted curves by Model I and Model II in Fig. 9, all the parameters were determined by the corresponding cyclic model, except that the actual unloading strain was adopted for each unloading cycle. It is also worth noting that the actual FRP rupture strain, which governs the failure of FRP-confined ECC, was adopted to determine the ultimate point for the test data obtained from Li et al. [22] [as shown in Figs. 9(a-f)]. However, for the test data obtained from Dang et al.

[21] [as shown in Figs. 9(g-l)], the actual hoop strain at FRP rupture was not reported. Instead, the actual ultimate compressive strength and ultimate axial strain were adopted for the specimens in Figs. 9(g-l).

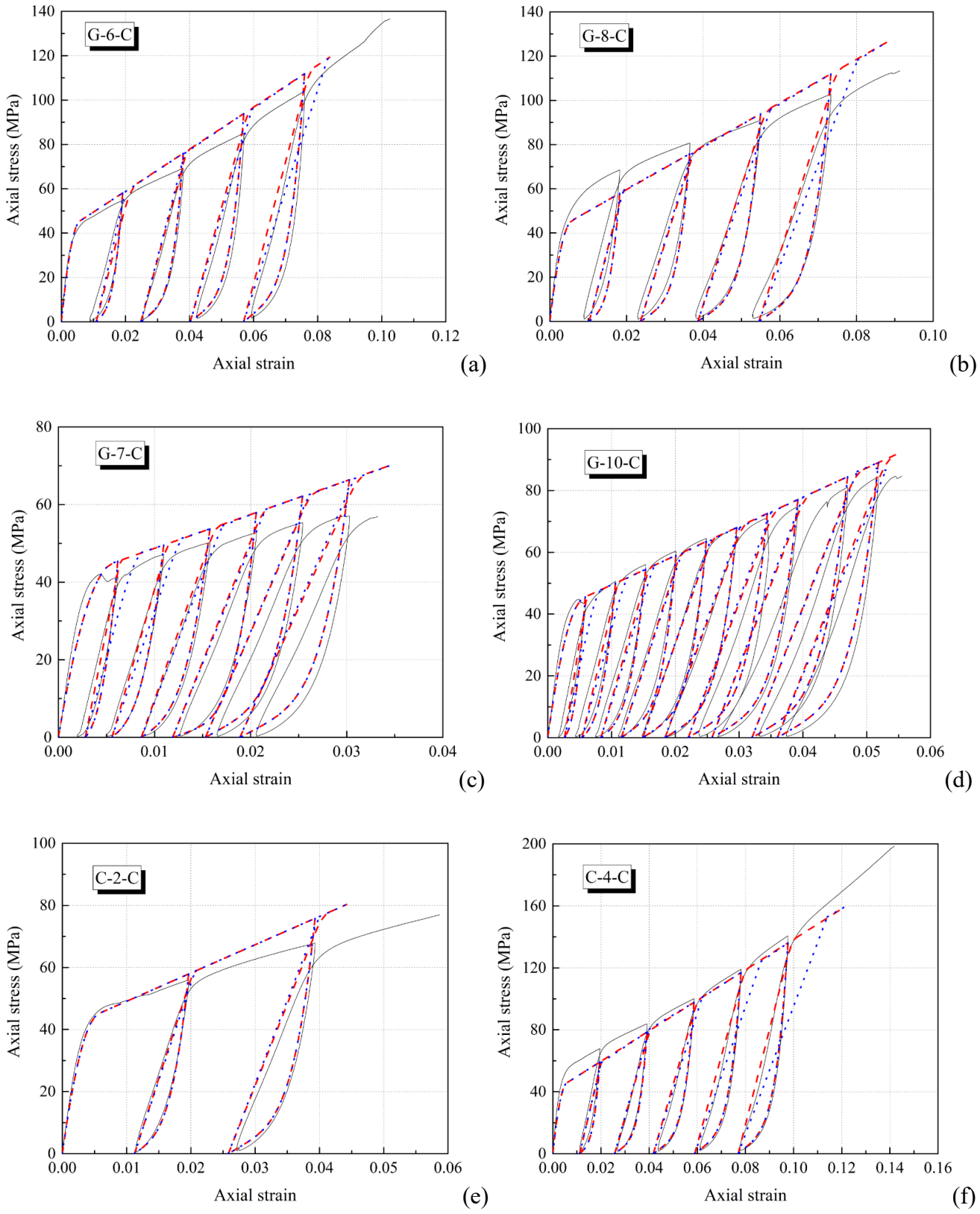

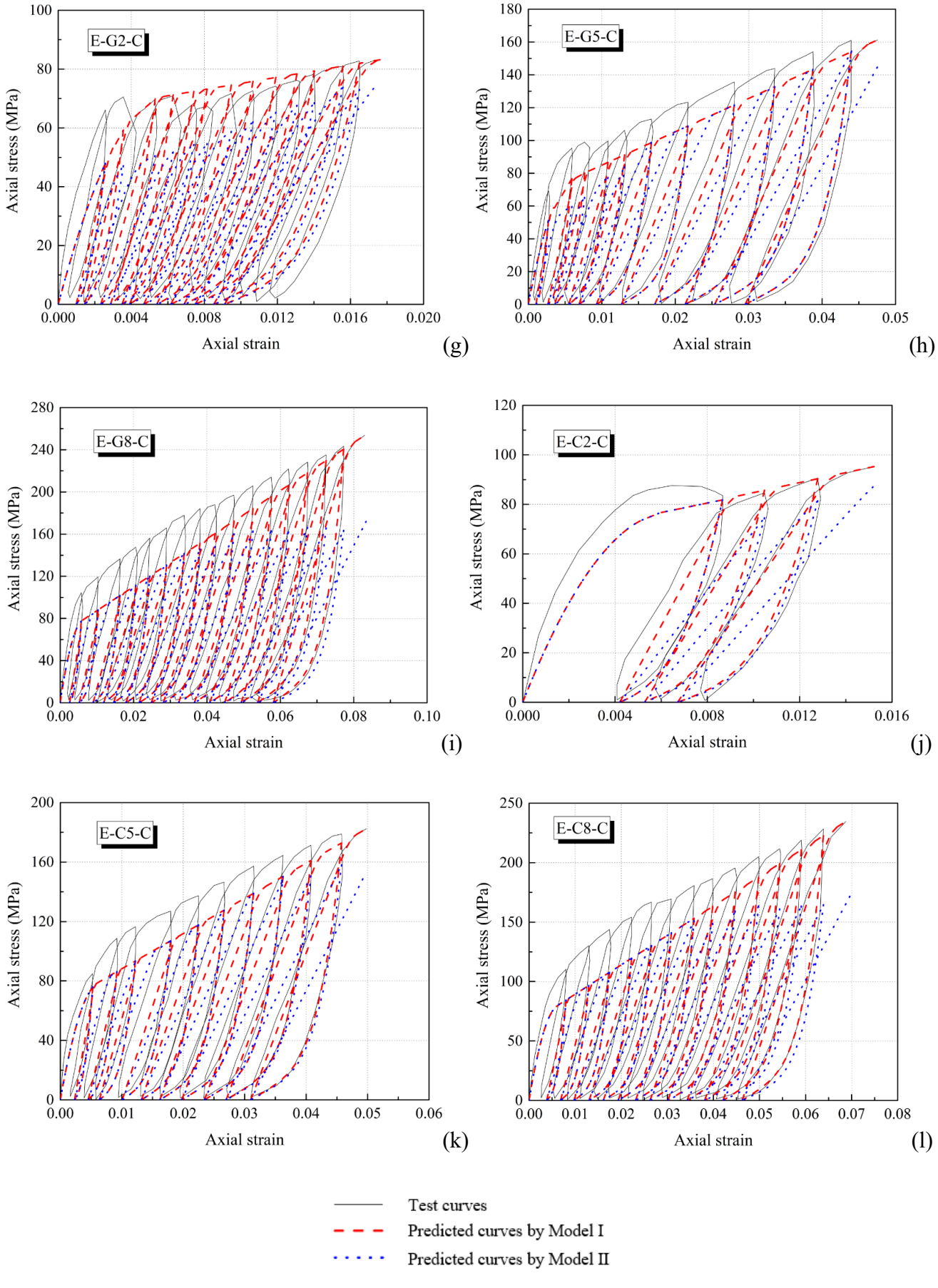

Fig. 9 Comparisons of cyclic stress-strain curves between test results and predicted results

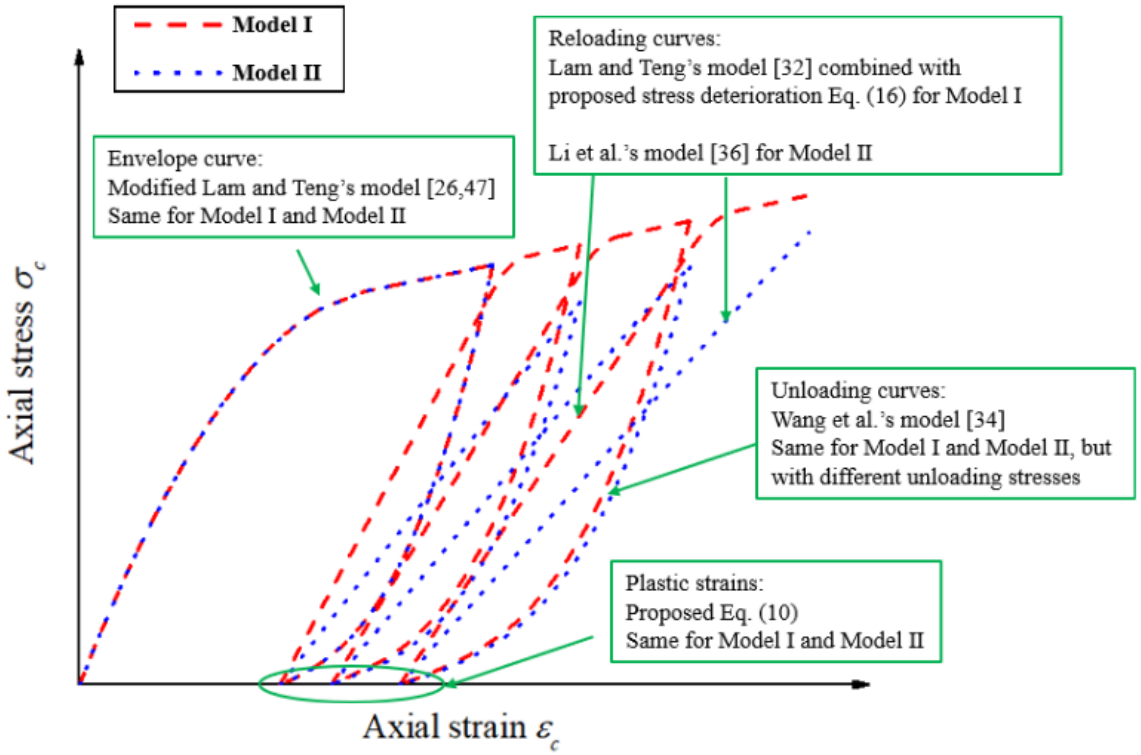

Fig. 10 Components in proposed Model I and Model II

In Figs. 9(a-f), the predicted results generated by Model I and Model II are with the same envelope curve, same unloading curves and different reloading curves, and the reloading curves generated by Model I are closer to the test reloading paths. In Figs. 9(g-l), the envelope curve, unloading curves and reloading curves generated by Model I and Model II are all different. For Model I predictions, the reloading curve always intersects with the envelope curve before reaching the next unloading strain, and the unloading stress was calculated with the envelope curve model at the corresponding unloading strain. For Model II predictions, however, the reloading curve may reach the next unloading strain before intersecting with the envelope curve, so that the unloading stress needs to be calculated with the reloading model at the corresponding unloading strain in this case. Meanwhile, the different unloading stress could also lead to different predicted unloading paths for Model I and Model II, though they are both using Wang et al.'s unloading model [34]. Overall, it can be observed from Fig. 9 that Model I outperforms Model II and provides closer predictions compared with the test results, especially in terms of the reloading paths. Therefore, the proposed Model I can be adopted for predicting the cyclic stress-strain behaviour of FRP-confined ECC to capture the envelope curve, unloading and reloading paths, plastic strains as well as stress deterioration behaviour. Furthermore, it also indicates that

406 the proposed Model I can provide acceptable predictions for cyclically loaded FRP-confined ECC with
407 different ECC strengths and confining stiffnesses.

408 It is noted that the relatively larger deviations between test curves and predicted curves can be observed for
409 the test specimens reported in Dang et al. [21], especially for the envelope curve for the specimens of "E-G5-
410 C", "E-G8-C", "E-C5-C" and "E-C8-C" as presented in Figs. 9(h, I, k and l). In Dang et al. [21], both
411 monotonic and cyclic test results on two identical specimens were reported, and the envelope curve of the
412 specimen under cyclic compression agreed well with the stress-strain curve of the counterpart specimen under
413 monotonic compression. In Li et al. [22], the monotonic test data collected from Dang et al. [21] were used to
414 develop the analysis-oriented model for FRP-confined ECC. It was observed that with the increase of
415 confining stiffness, some specimens presented the larger dilation behaviour and less strength enhancement
416 behaviour, which is not following the basic trend for FRP-confined concrete. Detailed discussions can be
417 referred to Li et al. [22]. Therefore, the test data from Dang et al. [21] may require further examination. It
418 could be the reason for the relatively larger deviations between test curves and predicted curves for the
419 specimens as shown in Figs. 9(h, I, k and l). On the other hand, the proposed cyclic models may also require
420 further validations with more test data in future studies.

421

422 **5. Conclusions**

423 This study presents the modelling of cyclic stress-strain behaviour of FRP-confined ECC. A database on FRP-
424 confined ECC was collected. Different components in cyclic stress-strain model of FRP-confined concrete,
425 including envelope curve, unloading and reloading paths, plastic strain and stress deterioration, were discussed
426 in detail. The applicability of existing models that were developed for FRP-confined normal concrete was
427 evaluated for FRP-confined ECC and new equations were also developed accordingly based on the test results
428 of FRP-confined ECC. The following conclusions can be obtained within the current scope of the study:

429 (1) Typical existing unloading and reloading models that were developed for FRP-confined normal
430 concrete were evaluated for FRP-confined ECC. Wang et al.'s model [34] was found to be able to
431 generate close predictions on the unloading behaviour of FRP-confined ECC. Lam and Teng's model

[32] and Li et al.'s model [36] could capture the characteristics of the reloading behaviour of FRP-confined ECC.

(2) Typical existing plastic strain models that were developed for FRP-confined normal concrete could not provide accurate predictions for FRP-confined ECC. Based on the available test data, new equation on plastic strain of cyclically loaded FRP-confined ECC was proposed. Meanwhile, new stress deterioration equation was also developed based on the test data for FRP-confined ECC under cyclic compression.

(3) Two cyclic stress-strain models, Model I and Model II, were proposed and used to predict the stress-strain curve for cyclically loaded FRP-confined ECC. Model I, which adopts modified Lam and Teng's envelope model [26,47] and Wang et al.'s unloading model [34] together with the newly proposed plastic strain model and stress deterioration model [Eqs. (10) and (16)] as well as Lam and Teng's reloading model [32], can provide close predictions compared with the test results and can be used as the cyclic stress-strain model for FRP-confined ECC.

This study presents the development approach to the cyclic stress-strain modelling of FRP-confined ECC. It is worth noting that the cyclic models presented in this study were developed based on the available test results of FRP-confined ECC under cyclic compression, which are the data obtained from Dang et al. [21] and Li et al. [22]. The unconfined ECC strengths are 40 MPa and 64.6-66 MPa. Meanwhile, the stress-strain curves are with the feature of an ascending second portion. Applicability of the proposed model is limited to these ranges and could be further verified with more cyclic FRP-confined ECC test data in future studies.

CRediT authorship contribution statement

Shuai Li: Investigation, Writing - original draft. **Tak-Ming Chan:** Writing - review & editing, Funding acquisition, Supervision. **Ben Young:** Writing - review & editing, Funding acquisition, Supervision.

Declaration of Competing Interest

The authors declare that they have no known competing financial interests or personal relationships that could have appeared to influence the work reported in this paper.

Acknowledgement

The research work presented in this paper was supported by the Research Grants Council of the Hong Kong Special Administrative Region, China – Theme-based Research Scheme (Project No. T22-502/18-R).

References

[1] Li VC. On engineered cementitious composites (ECC). J Adv Concr Technol 2003;1 (3):215–30.

[2] Xu LY, Huang BT, Li VC, Dai JG. High-strength high-ductility Engineered/Strain-Hardening Cementitious Composites (ECC/SHCC) incorporating geopolymer fine aggregates. Cem Concr Compos 2022;125:104296.

[3] Huang BT, Wu JQ, Yu J, Dai JG, Leung CKY, Li VC. Seawater sea-sand engineered/strain-hardening cementitious composites (ECC/SHCC): Assessment and modeling of crack characteristics. Cem Concr Res 2021;140:106292.

[4] Li VC, Wang S, Wu C. Tensile strain-hardening behavior of polyvinyl alcohol engineered cementitious composite (PVA-ECC). ACI Mater J 2001;98(6):483–92.

[5] Zhu JX, Xu LY, Huang BT, Weng KF, Dai JG. Recent developments in Engineered/Strain-Hardening Cementitious Composites (ECC/SHCC) with high and ultra-high strength. Constr Build Mater 2022;342:127956.

[6] Qin F, Zhang Z, Yin Z, Di J, Xu L, Xu X. Use of high strength, high ductility engineered cementitious composites (ECC) to enhance the flexural performance of reinforced concrete beams. J Build Eng 2020;32:101746.

[7] Yang X, Gao WY, Dai JG, Lu ZD, Yu KQ. Flexural strengthening of RC beams with CFRP grid-reinforced ECC matrix. Compos Struct 2018;189:9-26.

[8] Al-Gemeel AN, Zhuge Y. Using textile reinforced engineered cementitious composite for concrete columns confinement. Compos Struct 2019;210:695-706.

[9] Lee CK, Khan MKI, Zhang YX, Rana MM. Compressive performance of ECC-concrete encased high strength steel composite columns. Eng Struct 2020;213:110567.

[10] Khan MKI, Lee Ck, Zhang YX. Numerical modelling of engineered cementitious composites-concrete encased steel composite columns. J Constr Steel Res 2020;170:106082.

[11] Khan MKI, Lee Ck, Zhang YX, Rana MM. Compressive behaviour of ECC confined concrete partially encased steel composite columns using high strength steel. Constr Build Mater 2020;265:120783.

[12] Li S, Chan T-M, Young B. Experimental investigation on axial compressive behavior of novel FRP-ECC-HSC composite short column. Compos Struct 2023;303:116285.

[13] Li S, Chan T-M, Young B. Mechanical analysis and finite element modeling of FRP-ECC-HSC composite stub column under axial compression. J Build Eng 2022;62:105212.

[14] Li S, Chan T-M, Young B. Cyclic compressive behavior and load–strain model of FRP-ECC-HSC composite columns. J Struct Eng 2023;149(6):04023049.

[15] Li S, Chan T-M, Young B. Behavior of GFRP-concrete double tube composite columns. Thin Walled Struct 2022;178:109490.

[16] Li S, Chan T-M, Young B. Cyclic compressive behavior and load–strain model of FRP-concrete double tube composite columns. Thin Walled Struct 2023;184:110515.

[17] Li X, Li Y, Yan M, Meng W, Lu X, Chen K, Bao Y. Cyclic behavior of joints assembled using prefabricated beams and columns with Engineered Cementitious Composite (ECC). Eng Struct 2021;247:113115.

[18] Dong B, Pan J, Cai J, Xu L. Mechanical behaviour of a new ECC-encased CFST column to RC beam connection under cyclic loading. Eng Struct 2021;234:111915.

[19] Zhou J, Pan J, Leung CKY. Mechanical behavior of fiber reinforced engineered cementitious composites in uniaxial compression. J Mater Civ Eng 2015;27(1):04014111.

[20] Ding Y, YU K, Mao W. Compressive performance of all-grade engineered cementitious composites: Experiment and theoretical model. Constr Build Mater 2020;244:118357.

[21] Dang Z, Feng P, Yang JQ, Zhang Q. Axial compressive behavior of engineered cementitious composite confined by fiber-reinforced polymer. Compos Struct 2020;243:112191.

[22] Li S, Chan T-M, Young B. Compressive behavior and analysis-oriented model of FRP-confined engineered cementitious composite columns. Eng Struct 2022;270:114869.

[23] Yuan WY, Han Q, Bai YL, Du XL, Yan ZW. Compressive behavior and modelling of engineered cementitious composite (ECC) confined with LRS FRP and conventional FRP. Compos Struct 2021;272:114200.

[24] Yuan WY, Han Q, Bai YL, Song YC, Zhang Q. Size effect on compressive behavior of FRP-confined engineered cementitious composites (ECC). Constr Build Mater 2022;348:128610.

[25] Jiang J, Cui Y, Han Z. Experimental study and analysis-oriented model of PET FRP confined ECC cylinders under monotonic axial compression. Eng Struct 2023;280:115610.

[26] Li S, Chan T-M, Young B. Design-oriented stress-strain model for FRP-confined engineered cementitious composites. Eng Struct 2023;297:116983.

[27] Xu Y, Jia Y, Tong Z, Shivahari S. Cyclic loading test for concrete bridge columns integrated with ECC segment at the plastic zone. Eng Struct 2021;246:112985.

[28] Zhou Y, Wang X, Yuan F, Hu B, Zhu Z. Seismic retrofitting of coastal structural columns with steel bars locally corroded to fracture using sprayed ECC overlays and FRP jackets. Compos Struct 2023;307:116670.

[29] Huang CC, Hsiao H J, Shao Y, Yen CH. A comparative study on the seismic performance of RC beam-column joints retrofitted by ECC, FRP, and concrete jacketing methods. J Build Eng 2023;64:105691.

[30] Lam L, Teng JG, Cheung CH, Xiao Y. FRP-confined concrete under axial cyclic compression. Cem Concr Compos 2006;28(10):949–58.

[31] Shao Y, Zhu Z, Mirmiran A. Cyclic modeling of FRP-confined concrete with improved ductility. Cem Concr Compos 2006;28(10):959–968.

[32] Lam L, Teng JG. Stress–strain model for FRP-confined concrete under cyclic axial compression, Eng Struct 2009;31:308–321.

[33] Yu T, Zhang B, Teng JG. Unified cyclic stress–strain model for normal and high strength concrete confined with FRP. Eng Struct 2015;102:189-201.

[34] Wang Z, Wang D, Smith ST, Lu D. Experimental testing and analytical modeling of CFRP-confined large circular RC columns subjected to cyclic axial compression. Eng Struct 2012;40:64-74.

[35] Hany NF, Hantouche EG, Harajli MH. Axial stress-strain model of CFRP-confined concrete under monotonic and cyclic loading. J Compos Constr 2015;19(6):04015004.

[36] Li P, Wu YF, Zhou Y, Xing F. Cyclic stress-strain model for FRP-confined concrete considering post-peak softening. Compos Struct 2018;201:902-915.

[37] Bai YL, Mei SJ, Li P, Xu J. Cyclic stress-strain model for large-rupture strain fiber-reinforced polymer(LRS FRP)-confined concrete. J Build Eng 2021;42:102459.

[38] Zhou JK, Lin G, Teng JG. Compound concrete-filled FRP tubular columns under cyclic axial compression. Compos Struct 2021;275:114329.

[39] Zeng JJ, Liao J, Ye YY, Guo YC, Zheng Y, Tan LH. Behavior of FRP spiral strip-confined concrete under cyclic axial compression. Constr Build Mater 2021;295:123544.

[40] Bai YL, Dai JG, Ozbakkaloglu T. Cyclic stress-strain model incorporating buckling effect for steel reinforcing bars embedded in FRP-confined concrete. Compos Struct 2017;182:54-66.

[41] Ozbakkaloglu T, Lim JC. Axial compressive behavior of FRP-confined concrete: Experimental test database and a new design-oriented model. Compos Part B 2013;55:607-634.

[42] Yang J, and Feng P. Analysis-oriented models for FRP-confined concrete: 3D interpretation and general methodology. Eng Struct 2020;216:110749.

[43] Lai MH, Liang YW, Wang Q, Ren FM, Chen MT, Ho JCM. A stress-path dependent stress-strain model for FRP-confined concrete. Eng Struct 2020;203:109824.

[44] Dai JG, Bai YL, Teng JG. Behavior and modeling of concrete confined with FRP composites of large deformability. J Compos Constr 2011;15(6):963-973.

[45] Bai YL, Dai JG, Mohammadi M, Lin G, Mei SJ. Stiffness-based design-oriented compressive stress-strain model for large-rupture-strain (LRS) FRP-confined concrete. Compos Struct 2019;223:110953.

[46] Cavaleri L, Di Trapani, F, Ferrotto M F, Davì L. Stress-strain models for normal and high strength confined concrete: Test and comparison of literature models reliability in reproducing experimental results. Ingegneria Sismica, 2017;34(3):114 - 137.

[47] Lam L, Teng JG. Design-oriented stress-strain model for FRP-confined concrete. Constr Build Mater 2003;17(6):471–89.

[48] Teng JG, Jiang T, Lam L, Luo YZ. Refinement of a design-oriented stress–strain model for FRP-confined concrete. J Compos Constr 2009;13(4):269-278.

[49] Liao J, Zeng JJ, Gong QM, Quach WM, Gao WY, Zhang L. Design-oriented stress-strain model for FRP-confined ultra-high performance concrete (UHPC). Constr Build Mater 2022;318:126200.

[50] Chen G, Wang Y, Yu T, Wan B, Zhang B, Liu Q. Behavior and design-oriented model for elliptical FRP-confined concrete under axial compression. Eng Struct 2021;249:113387.

[51] Concrete Society, Design guidance for strengthening concrete structures with fibre composite materials, Technical Rep. No. 55, 3rd Ed., Crowthorne, Berkshire, U.K. 2012.

[52] American Concrete Institute ACI, Guide for the design and construction of externally bonded FRP systems for strengthening concrete structures, ACI-440 2R, Farmington Hills, Mich. 2017.